Applied Chemistry Today **20(77)** (2025) 49-68

Semnan University

Applied Chemistry Today

Journal homepage: https://chemistry.semnan.ac.ir/

ISSN: 2981-2437

Research Article

Theophylline-functionalized magnetic nanoadsorbent: synthesis, characterization, solid phase extraction of copper, modeling of isotherms and adsorption kinetics

Parvin Barashroudi[1], Majid Ghahraman Afshar[2,*], Niloufar Bahrami Panah[1], Abbas Maleki[1]

[1]*Department of Chemistry, Payame Noor University (PNU), Tehran, Iran*

[2]*Chemistry and Process Research Department, Niroo Research Institute (NRI), Tehran, Iran*

PAPER INFO

Article history:
Received: 03/May/2025
Revised: 24/Jul/2025
Accepted: 28/Jul/2025

Keywords:
Surface adsorption,
copper ion,
core-shell structure,
$Fe_3O_4@SiO_2$,
theophylline molecule,
Langmuir model,
Freundlich model.

ABSTRACT

In this study, $Fe_3O_4@SiO_2$ core-shell nanoparticles functionalized with theophylline molecules were synthesized and used as an effective and strong nanoadsorbent for the removal of divalent copper ions from aqueous solutions. The synthetic and structural steps of the nanoadsorbent, morphology and particle size were investigated using techniques such as Fourier transform infrared spectroscopy, X-ray diffraction, nitrogen gas adsorption-desorption, vibrating sample magnetometer, thermal analysis, scanning electron microscopy, transmission electron microscopy and particle size distribution. In order to evaluate the adsorption performance of nanadosorbent in removing copper ions, initially the optimization of nanoadsorbent dosage, solution pH, initial copper ion concentration and nanoadsorbent contact time were investigated and the results showed the best adsorption performance in the presence of 21 mg of synthetic nanoadsorbent, pH 7 in 75 mL of solution with initial concentration of 0.55 mmol/L at ambient temperature and contact time of 20 min. The adsorption isotherm followed the Langmuir model which resulted in a maximum adsorption capacity of copper ions of 134.7 mg/g. The calculated parameters indicated that the kinetic adsorption data were in well agreement with the pseudo-second-order kinetic adsorption model. This data confirmed that the chemisorption was the main rate-determining step. This synthetic nanoadsorbent is recovered with a magnetic field and reused in consecutive adsorption-desorption cycles for seven times without a noticeable decrease in adsorption activity.

DOI: https://doi.org/10.22075/chem.2025.37394.2360

[*]**. corresponding author:** Assistant Professor of Analytical Chemistry. *E-mail address: mghahramanafshar@nri.ac.ir*

How to cite this article: Barashroudi, P., Ghahraman Afshar, M., Bahrami Panah, N. & Maleki, A. (2025). Theophylline-functionalized magnetic nanoadsorbent: synthesis, characterization, solid phase extraction of copper, modeling of isotherms and adsorption kinetics. *Applied Chemistry Today*, **20(77)**, 49-68. (in Persian)

1. Introduction

The need to monitor and remove heavy metal ions is very important due to the various problems and issues that these metals create for human health and ecosystems. Therefore, various methods including biosorption, membrane processes, reverse osmosis, ion exchange, absorption, filtration, and sedimentation are applied to remove heavy metal ions from industrial effluents and waste water. Among all mentioned methods, the application of adsorption methods has attracted much attention due to advantages including economical synthesis, ability to remove low concentrations, high efficiency and the ability to use various biocompatible compounds [1-7].

Copper is one of the metal ions which is in excessive dose leads to complications such as impaired reading and writing, decreased blood pressure, nausea, increased heart rate, attention deficit disorder, ear infections and headaches. In addition, it leads to liver damage, anemia, hair loss, deposition in the liver and brain, symptoms of poisoning such as autism (personality changes, depression, insomnia, madness, hallucinations, paranoia) and schizophrenia. As a result, many studies have been conducted to remove copper ions considering the serious damage this metal ion causes to the metabolisms of living organisms recently [8-13].

Nowadays, adsorbents such as zeolites, magnetic composites, biomass, clay, carbon adsorbents (carbon nanotubes, chitosan, activated carbon) and polymer adsorbents have been interrogated in adsorption processes. Most of these adsorbents have disadvantages such as difficult synthesis, reduced activity in the adsorption process, difficult separation and low adsorption capacity. Therefore, the need to synthesize a novel, effective and powerful adsorbent for the removal of heavy metal ions from aqueous solutions is strongly required. Application of nanotechnology in the adsorption processes of heavy metal ions has received great attention recently [14-17].

Among all nanoparticles, Fe3O4 magnetic nanoparticles (MNPs) have attracted great attention due to their properties and wide applications in various fields. MNPs are applied as an nanoadsorbent, gas sensors, catalysts, ion exchangers, and magnetic resonance imaging. These nanoparticles are of great interest due to their properties such as low toxicity, high specific surface area, small particle size, excellent magnetic properties and the ability to be easily separated by an external magnetic field. However, MNPs have a high tendency to aggregate and accumulate which leads to a decrease in their activity [18-23].

Moreover, Magnetite nanoparticles are structurally degraded in acidic environments and oxidized in the presence of oxygen of the air. To overcome these issues, the use of coatings and surface stabilizers is crucial. The various nanocoating's including silica (Fe_3O_4@SiO_2), polymers (Fe_3O_4@Polymer), metal-organic frameworks (Fe3O4@MOF) and carbon (Fe_3O_4@Carbon) has received great attention in order to protect Fe_3O_4 nanoparticles and prevent them from agglomerating recently [24-29].

Among the mentioned coatings, the use of nanosilica as a coating has attracted much attention due to its special properties including the possibility of surface modification, easy functionalization, approximately similar particle size and high specific surface area. In core-shell structures, the surface atoms play a fundamental role and the central atoms do not play an effective functional role. The silica surface allows for functionalization for a variety of applications due to its abundant surface hydroxyl groups. Surface functionalization of nanoparticles provides distinct properties such as the ability to bind to biomolecules, surface hydrophobicity, and biocompatibility [30-33].

here in this research compared to previous studies conducted by this research group, new linkers (3-aminopropyltriethoxysilane, trichloro triazine and 3-aminopropyl) and theophylline as a novel ligand are used for the first time to functionalize core-shell nanoparticles. Theophylline ligand has oxygen and nitrogen heteroatoms which make it appropriate structure with the ability of chelating various types of heavy metal ions. On the other hand, by attaching this ligand to the core-shell structure, it is possible to adsorb heavy metal ions and ultimately separate them with an external magnet.

Another key feature of this ligand which is impossible in the previous research is the ability to harness the therapeutic properties of theophylline ligand in coupled with magnetic nanoparticles. Theophylline acts as a ligand with medical properties. The theophylline ligand is able to bind to a protein or other molecule in the body and alter its activity. Specifically, theophylline binds to the enzyme phosphodiesterase and inhibits the enzyme increases the level of cAMP in the cell. Theophylline is a bronchodilator of the methylxanthine class that relaxes the muscles of the chest and lungs to make breathing easier and reduces the sensitivity of the bronchi to allergens and other bronchospasm-causing agents. This medication is also used to treat shortness of breath and symptoms of asthma, bronchitis, emphysema, and other respiratory problems. Theophylline directly relaxes the smooth muscles of the airways and pulmonary vessels by increasing intracellular cAMP by reducing bronchospasm and increasing airflow velocity and vital capacity [34-39].

Among the specific applications proposed for this synthetic nanoparticle is the binding of theophylline to a non-toxic core-shell structure and its targeting to the target tissue. The pharmacological properties of the proposed ligand are among the key advantages and strengths of this research.

2. Experimental

Here in this research, $Fe_3O_4@SiO_2$ nanoparticles are first synthesized using coprecipitation and Stöber methods. In the next step, these nanoparticles are functionalized with 3-aminopropyl triethoxysilane, trichloro triazine, 3-bromopropylamine, and theophylline molecules, respectively. Finally, the synthesized nanoparticle is applied as an effective nanoadsorbent for the removal of copper ions from aqueous solutions. The structural, morphological, particle size and step-by-step synthesis of the nanoadsorbent are evaluated using XRD, FE-SEM, TEM, DLS, FT-IR, BET, EDX, TGA and VSM tests. Optimization of effective parameters including initial target ion concentration, adsorbent dosage, pH, adsorption isotherms, adsorption kinetics and adsorbent recovery are performed in the solid phase extraction (SPE) process. In order to achieve the optimal condition of SPE process, Langmuir and Freundlich kinetic isotherms are applied here. Therefore, two kinetic models (pseudo-first order and pseudo-second order) are used as common models in the study of adsorption kinetics.

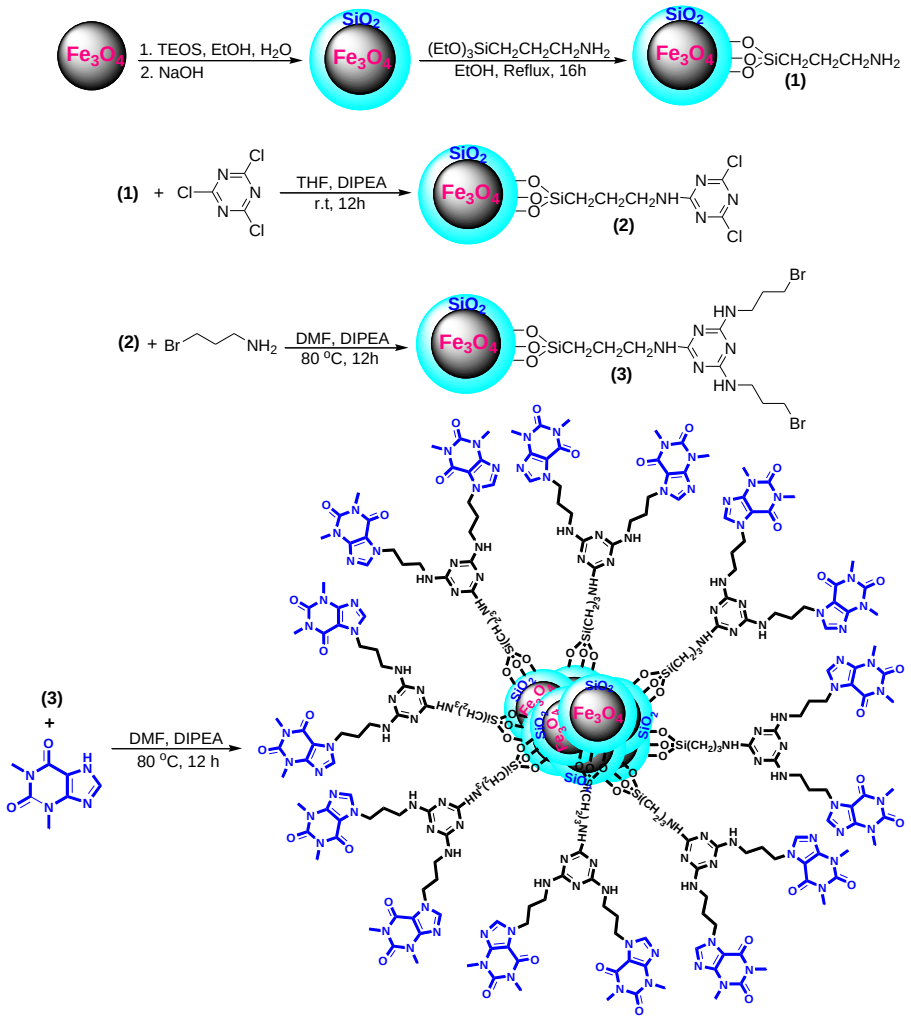

Scheme 1. Synthesis process of Fe_3O_4@SiO_2 nanoparticles functionalized with theophylline molecules.

2.1. Materials and Equipment

All applied chemicals for the synthesis and performance testing of the nanosorbent are purchased from Aldrich. The solvents are used without analytical purification. X-ray diffraction (XRD) analysis of the synthetic nanoparticles is performed using a Bruker AXS D8 instrument (CuKα radiation, λ= 1.5418nm) in a range of 2θ=10-80°. Fourier transform infrared spectroscopy (FT-IR) of the synthetic nanoparticles is performed using a Shimadzu FT-IR 8300 instrument. A scanning electron microscope (FE-SEM, Hitachi S-4160) and a transmission electron microscope (TEM, Philips EM208) with a voltage increase of 100 Kw are used to evaluate and investigate the morphology and size of the synthetic nanoparticles. The HORIBA-LB550 device is used to evaluate the particle size distribution. The specific surface area and porosity of the synthesized nanoparticles are investigated by nitrogen adsorption-desorption isotherm and using the Brunauer-Emmett-Teller (BET) method. Inductively coupled plasma (ICP) is used to determine the residual concentration of ions in the solution.

2.2. Synthesis of nanoadsorbent

2.2.1. Synthesis of magnetite nanoparticles (Fe_3O_4)

Fe_3O_4 nanoparticles are synthesized using the co-precipitation method. For this synthesis, 1 g of polyvinyl alcohol (PVA15000), 0.9 g of ferric chloride tetrahydrate and 1.3 g of ferric chloride hexahydrate are added to 60 mL of distilled water initially. After that, this mixture is subjected to intense mechanical rotation at 80 °C for 0.5 h. In the

next step, hexamethylenetetramine (1.0 mol/L) is added dropwise to the resulting mixture until the pH value reached to 10.

To complete the reaction and synthesize Fe_3O_4 nanoparticles, this mixture was subjected to mechanical rotation at 60 °C for 2 h. Finally, the synthesized magnetite nanoparticles are separated with an external magnetic field, washed several times with distilled water and ethanol, and finally dried at 80 °C for 10 h [40].

2.2.2. Synthesis of Fe_3O_4@SiO_2 core-shell nanoparticles

The Stöber method is used to synthesize Fe_3O_4@SiO_2 core-shell nanoparticles. For this synthesis, 0.5 g of magnetite nanoparticles and 0.2 mL of tetraethoxysilane are added to a mixture of 50 mL of ethanol and 5 mL of distilled water. In the next step, 5 mL of NaOH (10% w/w) is added dropwise to the mixture under mechanical rotation. This mixture is subjected to mechanical rotation for 0.5 h at ambient temperature. In the next step, the synthetic nanoparticles are separated by applying an external magnetic field. Finally, these nanoparticles are washed with distilled water and ethanol several times and dried for 10 h at 80 °C [41].

2.2.3. Synthesis of Fe_3O_4@SiO_2 core-shell nanoparticles functionalized with 3-aminopropyltriethoxysilane (Fe_3O_4@SiO_2-NH_2 MNPs)

To synthesize these nanoparticles, the core-shell nanoparticles are first sonicated in ethanol (10 mL) for 5 min to remove the aggregates and clumps. After that, 3-aminopropyltriethoxysilane (0.25 mL, 1 mmol) is added to it. In the next step, the resulting mixture is subjected to reflux and vigorous mechanical rotation for 16 h. Finally, the synthetic Fe_3O_4@SiO_2-NH_2 nanoparticles are separated using a magnet, washed with distilled water and ethanol several times and finally dried at 80°C for 6 h [42].

2.2.4. Synthesis of Fe_3O_4@SiO_2-NH_2 nanoparticles functionalized with trichlorotriazine (Fe3O4@SiO2-TCT)

One g of Fe_3O_4@SiO_2-NH_2 nanoparticles are added to 10 mL of tetrahydrofuran (THF), 0.17 mL of diisopropylethylamine (DEPEA, 1 mmol) and 0.185 g of trichlorotriazine (1 mmol). The mixture is subjected to mechanical rotation at room temperature for 12 h. Finally, the synthetic Fe_3O_4@SiO_2-TCT nanoparticles are separated with an external magnetic field, washed several times with hot ethanol to remove unreacted species and finally dried at 60 °C for 8 h [43].

2.2.5. Synthesis of Fe_3O_4@SiO_2-TCT magnetic nanoparticles functionalized with 3-bromopropylamine (Fe_3O_4@SiO_2-TCT-(CH2)3Br)

In order to synthesize these nanoparticles, 0.35 mL of DEPEA (2 mmol), 0.27 g of 3-bromopropylamine (2 mmol) and 1 g of Fe_3O_4@SiO_2-TCT nanoparticles are added to 10 mL of dimethylformamide. Furthermore, the resulting mixture is subjected to mechanical rotation at 80 °C for 12 h. Finally, the synthetic Fe_3O_4@SiO_2-TCT-$(CH_2)_3$Br nanoparticles are separated with a magnetic field and washed 3 times with 10 mL of ethanol each time and finally dried at 60 °C for 6 h.

2.2.6. Synthesis of Fe_3O_4@SiO_2-TCT-Theophylline nanoparticles

In order to synthesize Fe_3O_4@SiO_2-TCT-Theophylline nanoparticles, 1 g of Fe_3O_4@SiO_2-TCT-(CH_2)3Br nanoparticles are added to a mixture of 10 mL of dimethylformamide, 0.36 g of theophylline (2 mmol) and 0.36 g of DEPEA (2 mmol). Finally, the resulting mixture is subjected to mechanical rotation at 80 °C for 12 h. In the next step, the synthetic brown Fe_3O_4@SiO_2-TCT-Theophylline nanoparticles are separated with a magnetic separator and washed several times with hot ethanol to remove unreacted species. Finally, these nanoparticles are dried at 60 °C for 6 h.

2.3. Adsorption isotherms and time-dependent behavior of Fe_3O_4@SiO_2-TCT-Theophylline nanoadsorbent in copper ion adsorption

To investigate the copper ion adsorption process with the synthetic nanoadsorbent, the adsorption performance is evaluated using 21 mg of Fe_3O_4@SiO_2-TCT-Theophylline nanoadsorbent in 75 mL of copper ion solution with initial concentration 0.55 mmol/L at pH 7 and in a time interval of 4-24 min. The Fe_3O_4@SiO_2-TCT-Theophylline nanoadsorbent is separated using a magnet and washed several times with 1 M HCl, distilled water and ethanol. Finally, the synthesized nanoparticles are dried at 70 °C for 6 hours to be ready for use in sequential adsorption-desorption processes. The concentration of the remaining ions in the solution is measured using inductively coupled plasma (ICP) spectroscopy. The adsorbed amount of each ion q_e (mmol/g) i calculated using equation (1):

$$q_e = \frac{V}{W}(C_0 - C_e) \quad (1)$$

In this equation, C_0 and C_e are the initial and final concentrations of the target ions in the solution (mmol/L), W is the amount of Fe_3O_4@SiO_2-TCT-Theophylline nanoadsorbent, V is the volume of the solution (Liter), and q_e is the adsorption capacity (mmol/g). The experimental data obtained from this study are fitted with the Langmuir and Freundlich isotherm models. The linear form of the Langmuir and Freundlich isotherms is shown in equations (2) and (3).

$$\frac{1}{q_e} = \frac{1}{q_{max}} + \frac{1}{k_L q_{max}} \frac{1}{C_e} \quad (2)$$

$$Log\ q_e = Log\ K_F + \frac{1}{n} Log\ C_e \quad (3)$$

In these equations, K_L is the Langmuir constant, C_e is the equilibrium concentration of copper ions, q_e is the equilibrium adsorption amount of copper ions, q_m is the maximum adsorption capacity (mol/g), 1/n and K_F are the experimental constants affecting the adsorption process.

Kinetic adsorption tests are performed at ambient temperature and for a time period of 4-24 min at an initial concentration of 0.55 mmol/L (75 mL) and q_t (mg/g) is calculated using equation (4):

$$q_t = \frac{V}{W}(C_0 - C_t) \quad (4)$$

In equation (4), Ct (mg/g) represents the concentration of Cu(II) ions at time t. Equations (5) and (6) show the linear form of the pseudo-first-order and pseudo-second-order kinetic models:

$$Ln\ (q_e - q_t) = Ln\ (q_e) - K_1 t \quad (5)$$

$$\frac{t}{q_t} = \frac{1}{K_2 q_e^2} + \frac{t}{q_e} \quad (6)$$

In this equation, K_1 (min^{-1}) and K_2 (mg/gmin) are the rate constants for the pseudo-first and second order kinetic models, and q_t (mg/g) is the adsorption capacity at time t.

3. Results and Discussion

The theophylline ligand is a ligand with therapeutic properties for the treatment of respiratory diseases. Therefore, this ligand is placed on the nanomagnetic core and is transferred to the target tissue by creating magnetic fields to treat respiratory diseases. On the other hand, the presented ligand has a high ability to chelate heavy metal ions due to the presence of heteroatoms (oxygen and nitrogen) on its surface. Accordingly, by functionalizing the nanomagnetic cores with the theophylline ligand, the ideal chelating properties of this ligand and also the easy separation of magnetic cores from aqueous solutions is interrogated for water and wastewater treatment purposes.

3.1. Characterization of Fe_3O_4@SiO_2-TCT-Theophyline nanoadsorbent

Figure 1 shows the FT-IR spectra of the synthetic nanoparticles a) Fe_3O_4, b) Fe_3O_4@SiO_2, c) Fe_3O_4@SiO_2-NH_2, d) Fe_3O_4@SiO_2-TCT, e) Fe_3O_4@SiO_2-TCT-$(CH_2)3Br$ and f) Fe_3O_4@SiO_2-TCT-Theophylline. In all synthetic samples, the peaks of the bending vibrations of the O-H bond at

1620 cm^{-1}, the stretching vibrations of the O-H bond at 3400 cm^{-1} and the stretching vibrations of the Fe-O bond at 570 cm^{-1} are observed (Figure 1).

The presence of absorption peaks in the 1100 and 1800 cm^{-1} regions are related to the asymmetric and symmetric stretching vibrations of the Si-O-Si bond, respectively. These peaks confirm the surface coating of magnetite nanoparticles with a silica layer and the synthesis of $Fe_3O_4@SiO_2$ nanoparticles (Figure b1). The presence of absorption peaks in the regions 3170-3390, 2810-2986, 1543, 1489, 1123 and 576 cm^{-1} are assigned to N-H (stretching vibrations), C-H (stretching vibrations), N-H (bending), CH_2 (bending), Si-O-Si (asymmetric stretching vibrations) and Fe-O (stretching vibrations) bonds, respectively. These peaks indicate the functionalization of core-shell $Fe_3O_4@SiO_2$ nanoparticles with 3-aminopropyltriethoxysilane and the successful synthesis of $Fe_3O_4@SiO_2$-NH_2 nanoparticles (Figure c1).

After functionalization of $Fe_3O_4@SiO_2$-NH_2 nanoparticles with trichloro triazine (cyanuric chloride, TCT), new peaks are observed in the regions of 1711, 1564, 1511 cm^{-1} (stretching vibrations of the C=N bond) and 1226 cm^{-1} (stretching vibrations of the C-N bond). These peaks confirm the synthesis of $Fe_3O_4@SiO_2$-TCT nanoparticles (Figure d1). Moreover, the stretching vibrations of the C-Cl bond overlap with the broad and strong peak of the Si-O-Si bond (asymmetric stretching vibrations) at 1100 cm-1. The symmetric Si-O-Si stretching peak is a broad peak in the 1100 cm^{-1} region which covers the narrow peak of C-Cl stretching vibrations. For this reason, the C-Cl peak is not clearly visible in figure d1.

The successful synthesis of synthetic $Fe_3O_4@SiO_2$-TCT-$(CH_2)_3$Br nanoparticles is confirmed by the formation of new absorption peaks at 1327 and 1583 cm^{-1}. These peaks are assigned to the stretching vibrations of the C-N and C-Br bonds, respectively (Figure e1). Finally, the functionalization of $Fe_3O_4@SiO_2$-TCT-$(CH_2)_3$Br nanoparticles with theophylline molecules is confirmed by the presence of absorption peaks at 3441 (stretching vibrations of the O-H bond), 2847-3047 (stretching vibrations of the C-H), 1717 (stretching vibrations of the C=O), 1562, 1662 (stretching vibrations of the C=N of the trichloro triazine ring), 1396 (CH_3 bending vibrations), 1288 (C-N stretching vibrations), 1104 (Si-O-Si asymmetric stretching vibrations) and 1571 cm^{-1} (Fe-O bond stretching vibrations) are identified which is confirming the successful synthesis of $Fe_3O_4@SiO_2$-TCT-Theophylline nanoparticles (Figure f1).

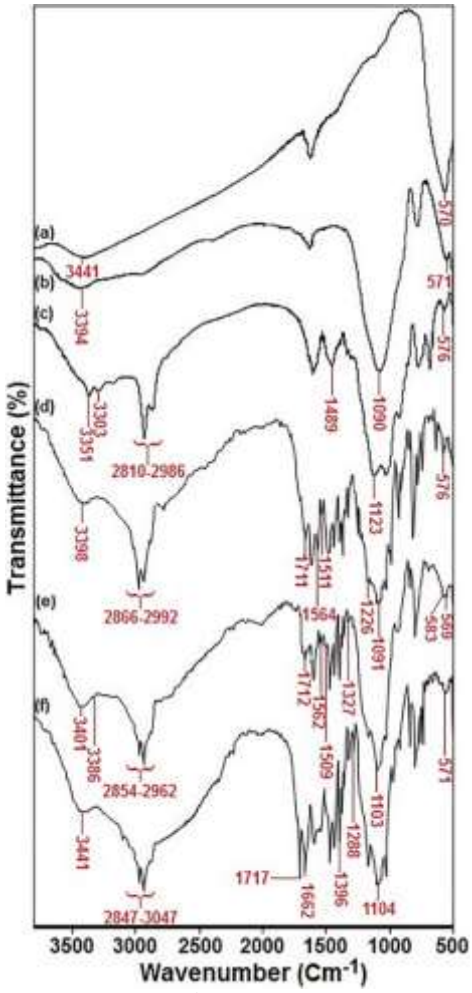

Figure 1. FT-IR spectra of synthetic nanoparticles a) Fe_3O_4, b) $Fe_3O_4@SiO_2$, c) $Fe_3O_4@SiO_2$-NH_2, d) $Fe_3O_4@SiO_2$-TCT, e) $Fe_3O4@SiO_2$-TCT-$(CH_2)3$Br and f) $Fe_3O_4@SiO_2$-TCT-Theophylline.

X-ray diffraction (XRD) is used to investigate the crystal structures of synthetic Fe_3O_4, Fe_3O_4@SiO_2 and Fe_3O_4@SiO_2-TCT-Theophylline nanoparticles. The presence of diffraction peaks at 2Θ angles of 62.6°, 57.0°, 53.4°, 43.1°, 43.5° and 30.1° are assigned to Miller indices (440), (511), (422), (400), (311) and (220), respectively. These peaks indicate the presence of Fe_3O_4 nanoparticles with a spinel structure with a cubic phase and in accordance with the JCPDS database No. 19-0629 (Figure 2). The intensity of the peaks is reduced without any change or shift in the diffraction angles of the peaks by coating and functionalizing the surface of Fe_3O_4 nanoparticles with a silica layer and organic molecules (Figures b, c2). In the X-ray diffraction of Fe_3O_4@SiO_2 nanoparticles, a broad peak is observed at the diffraction angles 2Θ=15-25° which is assigned to amorphous silica (Figure b2). This broad peak shifts to lower angles due to the interaction effect of amorphous silica and surface organic compounds since the functionalization of these nanoparticles with organic molecules increases (Figure 2c) [44].

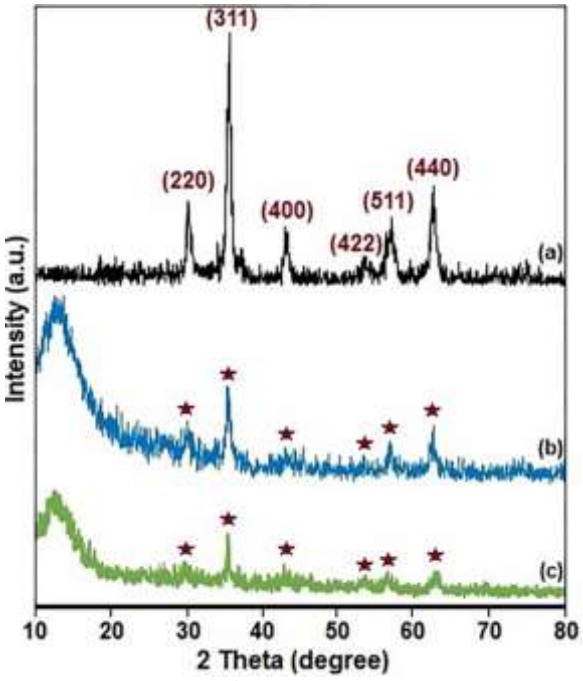

Figure 2. XRD spectra of synthetic nanoparticles a) Fe_3O_4, b) Fe_3O_4@SiO_2 and c) Fe_3O_4@SiO_2-TCT-Theophyline.

Transmission electron microscopy (TEM) images of the synthesized nanoparticles are shown in Figure 3a-c. Based on the TEM image of Fe_3O_4 nanoparticles, the average particle size of about 12 nm is observed. TEM image clearly shows the aggregation and agglomeration of the particles (Figure 3a). After the surface coating of Fe_3O_4 nanoparticles with a silica layer and the synthesis of Fe_3O_4@SiO_2 core-shell nanoparticles, the TEM image shows a uniform and regular distribution of particles with a size of about 20 nm (Figure 3b). Furthermore, the high-resolution TEM image clearly shows the surface coating of Fe_3O_4 nanoparticles with a silica layer and the spherical morphology of the synthetic Fe_3O_4@SiO_2 nanoparticles (Figure 3b). Figure 3c shows the TEM image of the Fe_3O_4@SiO_2-TCT-Theophyline nanoadsorbent. According to this image, the adsorbent nanoparticles have a particle size of 30 nm and an almost spherical structure. In Figure 3c, the magnetite nanoparticles are black in color and the silica coating layer and organic compounds are gray in color with high resolution.

Scanning electron microscopy (FE-SEM) is applied to investigate and evaluate the morphology of the synthetic nanoparticles (Figures 3 d-f). According to Figures 3 d,e, magnetite and core-shell Fe_3O_4@SiO_2 nanoparticles have an almost spherical morphology and good particle dispersion. The FE-SEM image of the synthetic nanoadsorbent is shown in Figure 3f which shows that then nanoadsorbent nanoparticles have a spherical shape and an average particle size of 30 nm with good dispersion. DLS analysis is used to investigate the size distribution of the synthetic particles as shown in Figure 3 g-i. Based on this analysis, the average particle sizes of Fe_3O_4, Fe_3O_4@SiO_2, and Fe_3O_4@SiO_2-TCT-Theophyline are obtained 12, 20, and 31 nm, respectively. These data set is consistent with the results of TEM analysis.

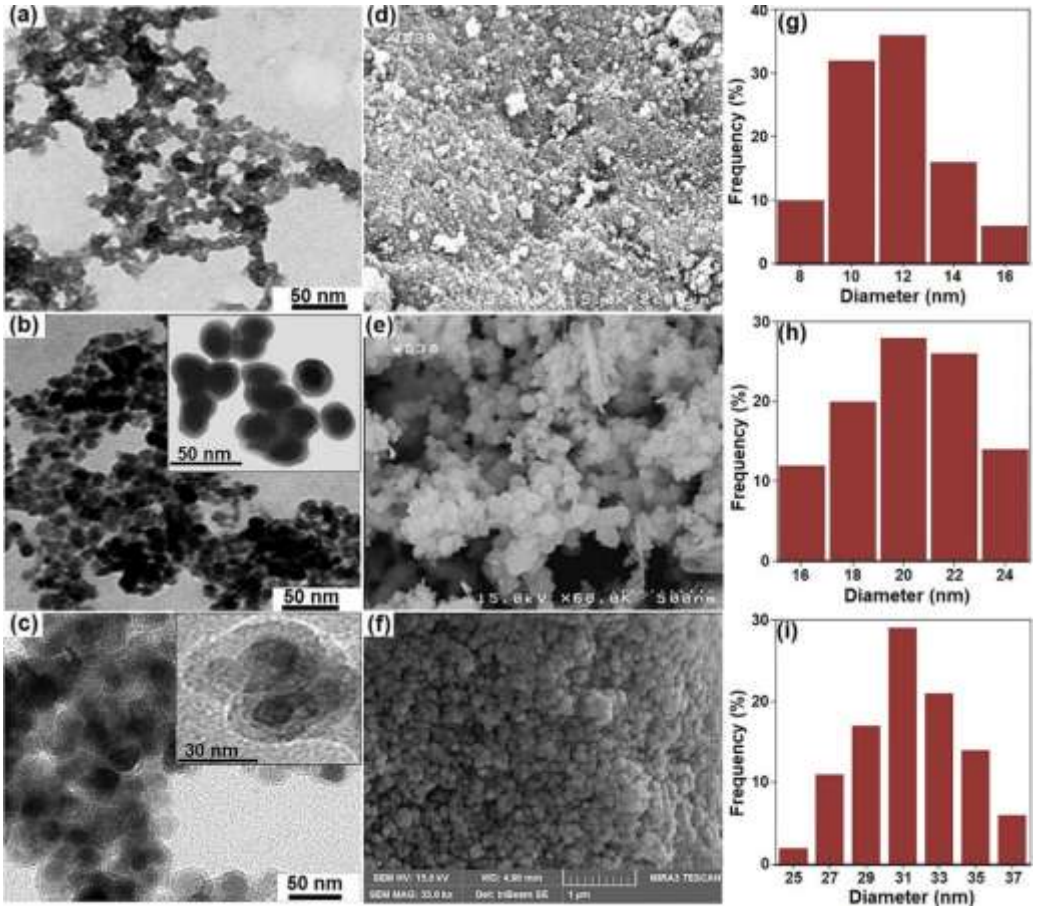

Figure 3. TEM, FE-SEM and DLS images for a), d) and g) Fe_3O_4, b), e) and h) Fe_3O_4@SiO_2, c), f) and i) Fe_3O_4@SiO_2-TCT-Theophyline nanoparticles, respectively.

The specific surface area and structural porosity of Fe_3O_4, Fe_3O_4@SiO_2 and Fe_3O_4@SiO_2-TCT-Theophylline nanoparticles are investigated using nitrogen gas adsorption-desorption. The results in Table 1 show that the specific surface area for these nanoparticles is 480, 430.3 and 392.6 m^2/g, respectively. Moreover, the results of Scherrer equation and transmission electron microscopy for the size of Fe_3O_4 particles in synthetic nanoparticles are summarized in Table 1. Based on Scherrer equation, the size of magnetite particles in synthetic nanoparticles Fe_3O_4, Fe_3O_4@SiO_2 and Fe_3O_4@SiO_2-TCT-Theophylline are 11.33 nm, 12.64 nm and 14.82 nm, respectively.

Table 1. Results of BET analysis for Fe_3O_4, Fe_3O_4@SiO_2, and Fe_3O_4@SiO_2-TCT-Theophyline nanoparticles.

Sample	Crystal Structure	Specific surface area (m^2/g)[a]	Particle diameter (nm)	
			XRD[b]	TEM[c]
Fe_3O_4	Cubic Spinel	480.0	11.33	12
Fe_3O_4@SiO_2	Cubic Spinel	430.3	12.64	20
Fe_3O_4@SiO_2-TCT-Theophylline	Cubic Spinel	392.6	14.82	30

a) Calculated by BJH
b) Calculated by Scherer equation based on XRD
c) Average particle size by using TEM image

The presence of iron, silica, oxygen, nitrogen, and carbon elements in the energy dispersive X-ray (EDX) analysis of the Fe_3O_4@SiO_2-TCT-Theophyline nanoadsorbent confirms the successful synthesis of this nanostructure (Figure 4a).

For investigation the thermal stability of the synthetic nanoparticles, thermogravimetric analysis (TGA) is interrogated as shown in Figure 4b.

According to this analysis, two weight loss stages are observed in the temperature range of 0-700 °C for the nanoparticles: a) Fe_3O_4@SiO_2-NH_2, b) Fe_3O_4@SiO_2-TCT, c) Fe_3O_4@SiO_2-TCT-(CH_2)3Br and d) Fe_3O_4@SiO_2-TCT-Theophylline. The weight loss below 200 °C is related to the evaporation of organic solvents and water while the weight loss above 200 °C is attributed to the removal of organic molecules from the surface of the Fe_3O_4@SiO_2 core-shell nanoparticles. TGA analysis of Fe_3O_4@SiO_2-TCT-Theophylline nanoadsorbent shows a maximum weight loss at 526 °C in the temperature range of 150-670 °C. this phenomena is resulting in a weight loss of 40.25% which is attributed to the thermal decomposition of organic compounds and theophylline molecules [45].

When the initial temperature is increased to 150°C, all volatile compounds such as water and organic solvents evaporate and a first weight loss step is observed at this temperature. When the temperature is increased to 350°C, all organic compounds containing carbon, nitrogen and hydrogen are converted to CO2, NO2 and H2O respectively. Accordingly, the binders and the theophylline compound are completely decomposed at a temperature of 350°C. Therefore, what remains are inorganic compounds or mineral ash at temperatures above 350°C.

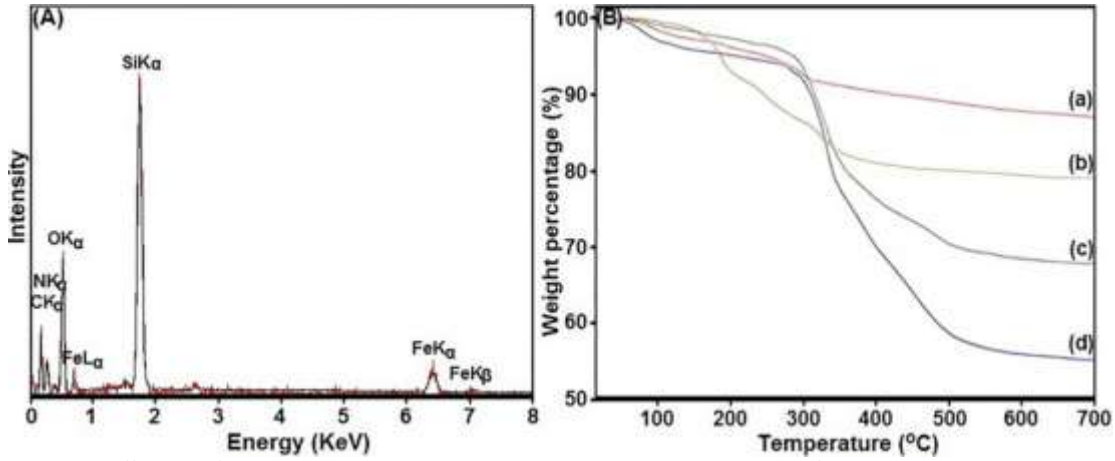

Figure 4. EDX diffraction of Fe_3O_4@SiO_2-TCT-Theophylline nanoparticles, B) TGA analysis of nanoparticles a) Fe_3O_4@SiO_2-NH_2, b) Fe_3O_4@SiO_2-TCT, c) Fe_3O_4@SiO_2-TCT-(CH_2)3Br and d) Fe_3O_4@SiO_2-TCT-Theophylline.

The VSM plots of the synthetic Fe_3O_4, Fe_3O_4@SiO_2 and Fe_3O_4@SiO_2-TCT-Theophyline nanoparticles at 300°K and a magnetic field of 8 KOe are shown in Figure 5a. Based on the VSM results, the saturation magnetization for these nanoparticles is 64.8, 40.3 and 32.1 emu/g, respectively. The saturation magnetization decreases with increasing weight and surface coating of Fe_3O_4 nanoparticles with a silica layer (Figure a-b). The magnetization property decreases to 32.1 emu/g with further functionalization of the Fe_3O_4@SiO_2 core-shell nanoparticles and the increase of non-magnetic components on the structure of these nanoparticles (Figure 5 a-b). However, the synthetic Fe_3O_4@SiO_2-TCT-Theophyline nanoadsorbent still exhibits a suitable saturation magnetic property which allows the separation from the solution using a magnetic field (Figure 5b).

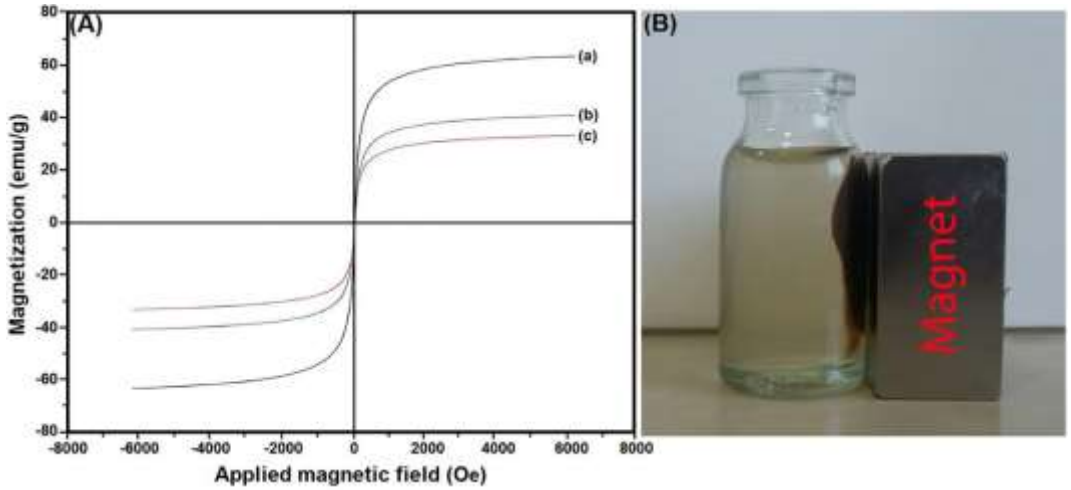

Figure 5. VSM diagram of synthetic nanoparticles a) Fe_3O_4, b) Fe_3O_4@SiO_2 and Fe_3O_4@SiO_2-TCT-Theophyline, B) Image of separation of Fe_3O_4@SiO_2-TCT-Theophyline nanosorbent with magnet.

3.2. Evaluation the performance of MNPs in the adsorption of copper

3.2.1. Optimization of the adsorbent amount

To optimize the amount of nanoadsorbent Fe_3O_4@SiO_2-TCT-Theophyline in the adsorption of divalent copper ions, studies were carried out in a range of 3-24 mg of adsorbent, pH 7 in 75 mL of solution with an initial concentration of copper ions of 0.55 mmol/L at ambient temperature for 30 minutes. As it is observed from figure 6, the absorption of divalent copper ions from the solution increases with increasing the dose of nanoadsorbent. The maximum adsorption of 96% obtained with the use of 21 mg of nanoadsorbent. The use of higher amounts of nanoadsorbent more than 24 mg is not lead to an increase the absorption of target ions. The number of active sites of the increases with increasing the amount of nanoadsorbent. On the other hand, a higher dose of nanoadsorbent more than 24 mg does not have much effect on the absorption amount considering the constant concentration of copper ions in the solution.

3.2.2 Optimization of pH

The pH of the solution plays a fundamental role in determining the dominant form of metal ions and changes in the surface charge of the nanoadsorbent among all important factors in the adsorption process.

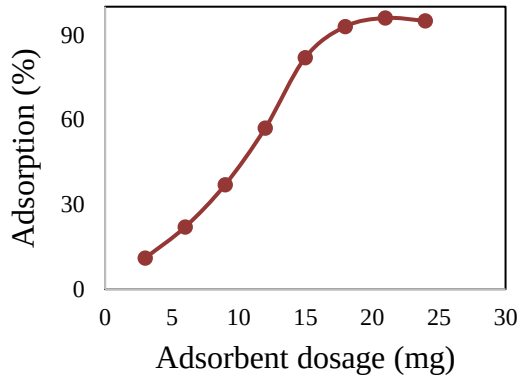

Figure 6. Effect of Fe3O4@SiO2-TCT-Theophyline nanoadsorbent dosage on copper ion adsorption.

Therefore, the changes in solution pH are investigated in the range of 3-8 in the presence of 21 mg of Fe_3O_4@SiO_2-TCT-Theophyline nanoadsorbent in 75 mL of copper solution with initial concentration 0.55 mmol/L at ambient temperature (Figure 7). Due to the protonation of the active sites of the nanoadsorbent at lower pH than 6, the reduction of the coordination strength occurs. This effect diminishes the coordination of nanoadsorbent with copper ions and leads to decrease the adsorption rate. The adsorption rate increases around pH 7 and the maximum adsorption capacity obtained at this pH.

The main reason for the decrease in metal ion adsorption at pH values above 7 is attributed to the increase in the concentration of hydroxyl ions. At pH values above 7, the concentration of hydroxyl

ions increases which result in increasing the tendency of hydroxyl ions to form hydroxyl salts with copper ions. As a result of the formation of hydroxyl copper salts, the concentration of free copper ions decreases. Due to the decrease in the concentration of free copper ions, the degree of copper coordination decreases despite the availability of theophylline active sites. At pH above 7, the concentration of free copper ions decrease compared to total copper ion. As the pH increases, the concentration of free copper ions also follows a decreasing trend.

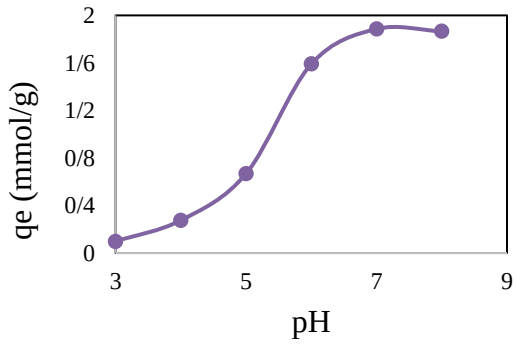

Figure 7. Optimization of solution pH on the adsorption rate of Fe_3O_4@SiO_2-TCT-Theophyline nanoadsorbent.

3.2.3. Optimization of the initial concentration of copper ions

To evaluate the effect of initial concentration of copper ions on the adsorption rate, experiments are carried out in a concentration range of 0.1-0.6 mmol/L of copper ion solution (75 ml) in the presence of 21 mg of nanoadsorbent at pH 7 with a contact time of 30 min. According to the figure 8, the maximum adsorption capacity is observed at concentration range of 0.55 mmol/L. Improvement in adsorption efficiency is observed with increasing initial concentration of copper ion which is attributed to the increase in mass gradient between copper ion solution and Fe_3O_4@SiO_2-TCT-Theophyline nanoadsorbent.

3.2.4. Optimization of the contact time of Fe_3O_4@SiO_2-TCT-Theophyline

In order to investigate the contact time of Fe3O4@SiO_2-TCT-Theophyline adsorbent in the adsorption of copper ions, 75 ml of copper ion solution with initial concentration of 0.55 mmol/L and 21 mg of nanoadsorbent are used at ambient temperature and pH 7.

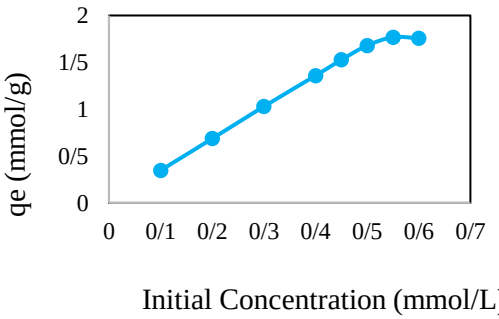

Figure 8. Effect of initial concentration of copper ions on the adsorption rate of Fe_3O_4@SiO_2-TCT-Theophyline adsorbent.

3.2.4. Optimization of the contact time of Fe_3O_4@SiO_2-TCT-Theophyline

In order to investigate the contact time of Fe3O4@SiO_2-TCT-Theophyline adsorbent in the adsorption of copper ions, 75 ml of copper ion solution with initial concentration of 0.55 mmol/L and 21 mg of nanoadsorbent are used at ambient temperature and pH 7. According to figure 9, the adsorption rate increases with increasing contact time. The highest adsorption rate occurs after 20 min. At the beginning of the adsorption process, the adsorption rate is gradually decreases with the saturation of the active sites by copper ions due to the abundance of active sites of the nanoadsorbent.

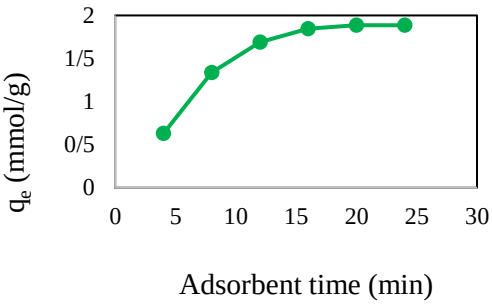

Figure 9. Optimization of the nanoadsorbent contact time in the adsorption of copper ions.

3.2.5. Recyclability and Reusability of Fe_3O_4@SiO_2-TCT-Theophyline Adsorbent

The ability to recover and reuse the nanoadsorbent in successive adsorption-desorption cycles are the most important factor among all factors in the

adsorption processes due to economic aspects. For this purpose, this nanoadsorbent is separated with a magnet and washed with 0.1 mol/L HCl and finally dried at 70 ºC for 5 hours after using Fe_3O_4@SiO_2-TCT-Theophyline in the removal of copper ions from aqueous solutions. In the next step, the usability of this nanoadsorbent in sequential processes is investigated. The results indicated that after 7 consecutive uses of this nanoadsorbent in adsorption-desorption processes, no noticeable decrease in the functional activity of the adsorbent was observed (Figure 10).

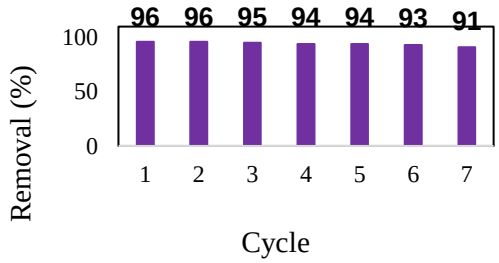

Figure 10. Evaluation of the adsorption of divalent copper ions using the Fe_3O_4@SiO_2-TCT-Theophyline nanoadsorbent in sequential adsorption-desorption processes.

3.3. Thermodynamic and kinetic model of copper ion adsorption

3.3.1. Adsorption isotherms

The isotherm diagram of copper ion in the presence of Fe_3O_4@SiO_2-TCT-Theophyline nanoadsorbent is shown in Figure 11. The initial fast slope indicates the high affinity of the nanoadsorbent for adsorption of copper ions.

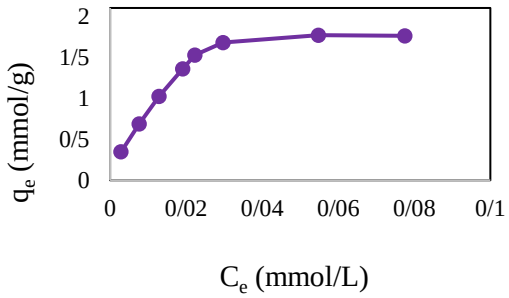

Figure 11. Adsorption isotherm of copper ions in the presence of Fe_3O_4@SiO_2-TCT-Theophyline adsorbent.

To evaluate the adsorption mechanism of copper ions by this nanoadsorbent, two Freundlich and Langmuir adsorption models are fitted to the experimental data [46]. The results of the studies are shown in figure 12.

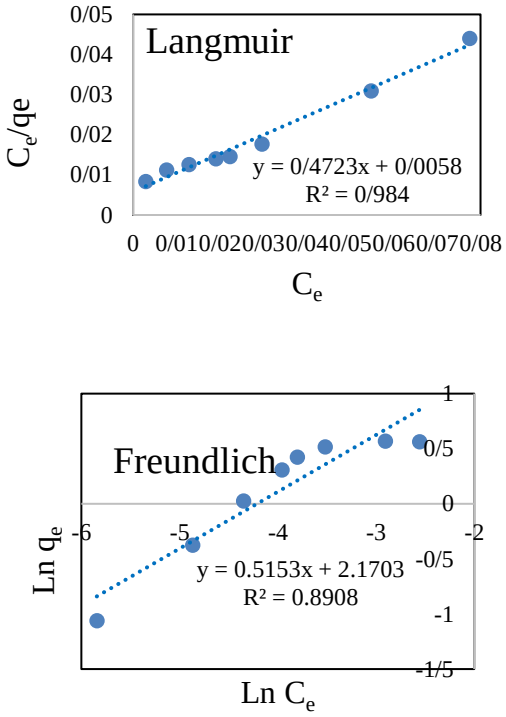

Figure 12. Langmuir and Freundlich models for the adsorption of copper ions by Fe_3O_4@SiO_2-TCT-Theophyline nanoadsorbent.

Table 2 shows the results of the effective parameters of the Langmuir and Freundlich isotherm models. These data sets confirm the homogeneous monolayer adsorption of copper ions on the nanoadsorbent surface due to the higher R_2 values in the Langmuir isotherm model. According to the Langmuir model, the maximum adsorption capacity (q_m) of the Fe_3O_4@SiO_2-TCT-Theophyline nanosorbent in the adsorption of taregt ions is 2.12 mmol/g.

Table 2. Langmuir and Freundlich isotherm model parameters.

Ion	Longmire model			Fredrich model		
	q_m (mmol/g)	K_L (L/mmol)	R^2	n	K_F (mmol/g)	R^2
Cu(II)	2.12	81.43	0.984	1.94	8.84	0.891

3.3.2. Adsorption Kinetics

To achieve the optimal time for the adsorption of target ions in the adsorption process, kinetic isotherms are applied here. As a result, two kinetic models including pseudo-first order and pseudo-second order are used as common models in the study of adsorption kinetics. The removal of copper ions occurs with a faster slope and the best adsorption performance after 20 min due to the abundance of nanoadsorbent active sites in the early times of the adsorption process.

Figure 13 shows the pseudo-first-order and pseudo-second-order kinetics diagrams for the adsorption of target ions in the presence of Fe_3O_4@SiO_2-TCT-Theophyline nanoadsorbent. A better agreement is observed between the data and the pseudo-second-order kinetic model according to the pseudo-first-order and pseudo-second-order kinetic parameters and R_2 values in Table 3. This kinetic model indicates the electrostatic adsorption and chemisorption mechanisms by the nanoadsorbent [47].

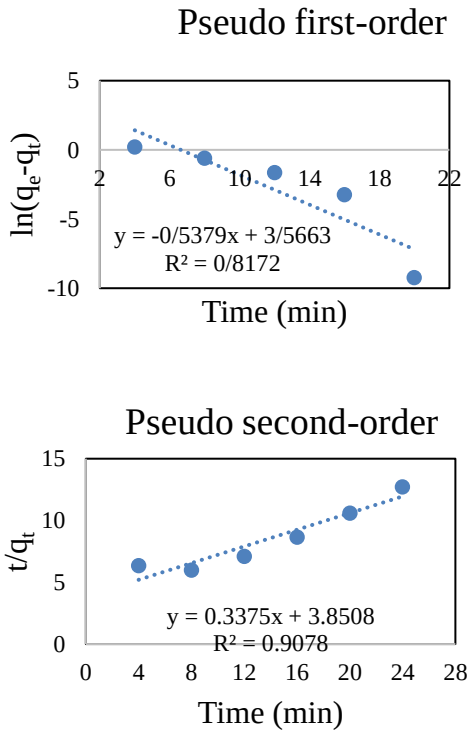

Figure 13. Pseudo-first-order and pseudo-second-order kinetic diagrams for the adsorption of copper ions with Fe_3O_4@SiO_2-TCT-Theophyline nanoadsorbent.

Table 3. Kinetic parameters in the adsorption of copper ions in the presence of Fe_3O_4@SiO_2-TCT-Theophyline nanoadsorbent.

Ion	Semi First-Order			Semi Second-Order		
	q_e (mmol /g)	K_1 (mi n^{-1})	R^2	q_e (mmol /g)	K_2 (g/mmol. min)	R^2
Cu(II)	35.9	0.538	0.817	2.963	0.0296	0.908

3.4. Comparison of various nanoadsorbents with Fe_3O_4@SiO_2-TCT-Theophyline

To investigate the adsorption performance of the synthetic nanoadsorbent with various adsorbents in scientific papers, the maximum adsorption capacity of these nanoadsorbents is evaluated and compared. Based on the results in table 4, the maximum adsorption capacity of Fe_3O_4@SiO_2-TCT-Theophyline is 134.7 mg/g which shows a significant performance compared to the other adsorbents. Moreover, this adsorbent has features such as high adsorption rate, low adsorbent amounts, excellent coordination with target ions, magnetic separation, and excellent adsorption performance in sequential processes which distinguish it from many other adsorbents.

Table 4. Comparison of the maximum adsorption capacity of the synthetic nanosorbent Fe_3O_4@SiO_2-TCT-Theophyline with various adsorbents in scientific articles in the adsorption of copper ions.

Adsorbent	Target	Ads. Capacity (mg/g)	Ref.
Nickel-ferrite/montmorillonite		18.7	[48]
Nano TiO_2	Cu(II)	10.0	[49]
1,5-Diphenylcarbazon/TiO_2 NPs	Cu(II)	25.5	[50]
MWCNTs–IDA	Cu(II)	6.6	[51]
Iron oxide NPs	Cu(II)	19.3	[52]
Fe_2O_3 nanoparticles-immobilized-sand	Cu(II)	5.8	[53]
Iron oxide coated sewage sludge	Cu(II)	17.3	[54]
Fe_3O_4@SiO_2-TCT-Theophyline	Cu(II)	134.7	**Presented**

4. Conclusion

In the present study, Fe_3O_4@SiO_2 core-shell nanoparticles are synthesized using coprecipitation and Stöber methods by functionalization with 3-aminopropyltriethoxysilane, trichlorotriazine, 3-bromopropylamine and theophylline molecules. The presented MNPs are used as an effective

nanoadsorbent for the removal of divalent copper ions from aqueous solutions. This nanoadsorbent with excellent magnetization capability allows for easy and convenient separation from the solution by using a magnet to remove the target ions. The results of the studies show that the rate of copper ion adsorption by the nanoadsorbent is strongly dependent on the pH. At low pHs, the rate of adsorption decreases due to the inactivation of heteroatomic groups and the reduction in the coordination ability of these active species with copper ions. The best adsorption performance of the synthetic nanoadsorbent occurs at pH 7 and the presence of 21 mg of Fe_3O_4@SiO_2-TCT-Theophyline nanoadsorbent which result in the removal of 96% of copper ions from the solution.

Investigations show that the adsorption process follows the Langmuir model and the adsorption kinetics follows the pseudo-second-order adsorption model. This synthetic nanoadsorbent is due to its outstanding characteristics including maximum adsorption capacity (134.7 mg/g), excellent coordination ability due to the abundance of hydroxy and nitrogen groups, high surface area to volume ratio (high specific surface area), the use of small amounts of adsorbent in the target ion absorption process, easy filtration with a magnetic field, the ability to recover and reuse in successive adsorption-desorption cycles enable its use as an effective and cost-effective adsorbent in the absorption of target ions from municipal and industrial wastewaters and effluents.

The proposed compound has the potential to be used in the treatment of respiratory diseases due to the special applications of theophylline. In this research, by functionalizing the nanomagnetic structure, the magnetic nanoparticle functionalized with theophylline molecules can be guided to the target tissue by creating an external magnetic field. Moreover, considering the special function of theophylline in adsorbing heavy metal ions, nanoparticles functionalized with theophylline molecules are applied to remove heavy metals from water and wastewater samples. Finally, the functionalized nanoparticles are separated using magnetic drums at the outlet of the treatment plant.

5. Acknowledgements

The authors of the article would like to express their gratitude to the chemistry department of Payam Noor University (PNU) and the chemistry and process department of Niroo Research Institute (NRI) for financial support and creating a suitable scientific environment.

References

[1] Özdemir S, Yalçın MS, Kılınç E. (2021). Preconcentrations of Ni (II) and Pb (II) from water and food samples by solid-phase extraction using Pleurotus ostreatus immobilized iron oxide nanoparticles. *Food Chemistry*. 336:127675.

[2] Ghahraman Afshar M ,Esmaeilpour M, Kazemnejadi M, Yousefpour A. (2024). Fe3O4@ SiO2 nanoparticles functionalized with glucosamine molecules as an effective and recyclable magnetic adsorbent to remove Zn2+. *Iranian Chemical Engineering Journal*.

[3] Esmaeilpour M, Ghahraman Afshar M. (2023). Magnetic Nanoadsorbent: Preparation, characterization, and Adsorption Properties for Removal of Copper (II) from Aqueous Solutions. *Applied Chemistry Today*. 18(69):11-20. (in persian)

[4] Li H, Jia Y, Chen Y, Ye Q, Xian L, Qian J. (2025). Amino-functionalized Yolk-shell Magnetic Silica Nanoparticles for the Selective Removal of Heavy Metal Ions. *Microporous and Mesoporous Materials*.113535.

[5] Akhter F, Pinjaro MA, Ahmed J, Ahmed M, Arain HJ, Ahsan MJ, et al. (2025). Recent advances and synthesis approaches for enhanced heavy metal adsorption from wastewater by silica-based and nanocellulose-based 3D structured aerogels: a state of the art review with adsorption mechanisms and prospects. *Biomass Conversion and Biorefinery*. 15(5):6585-614.

[6] Ghahraman Afshar M, Rajabi M, Payehghadr M, Bahrami Panah N. (2024). Fe3O4@ SiO2 Magnetic Core-Shell Nanoparticles Functionalized with 1, 4-dihydroxyanthraquinone as an Effective and Recyclable Adsorbent for Removal of Copper Ion from Aqueous Solutions. *Applied Chemistry Today*. 19(73):123-38. (in persian)

[7] Layeghi A, Payehghadr M, Afshar MG, Panah NB. (2023). Fe3O4@ SiO2 magnetic core-shell nanoparticles functionalized with-1, 4dihydroxyanthraquinone as an effective and recyclable adsorbent for the removal of divalent cadmium from aqueous solutions. *Journal of Applied Research of Chemical-Polymer Engineering*. 7(3):3-17.

[8] Nolan EM, Lippard SJ. (2008). Tools and tactics for the optical detection of mercuric ion. *Chemical reviews*. 108(9):3443-80.

[9] Niknam E, Ghahraman Afshar M, Ghaseminejad H, Esamaeilpour M. (2022). Pharmaceutical Pollutants Removal by Using Electrochemical Oxidation Technique. *Journal of Water and Wastewater; Ab va Fazilab (in persian)*. 33(4):71-81.

[10] Rao MM, Ramana D, Seshaiah K, Wang M, Chien SC .(۲۰۰۹) .Removal of some metal ions by activated carbon prepared from Phaseolus aureus hulls. *Journal of hazardous materials*. 166(2-3):1006-13.

[11] Soleimani M, Afshar MG. (2013). Potentiometric sensor for trace level analysis of copper based on carbon paste electrode modified with multi-walled carbon nanotubes. *International Journal of Electrochemical Science*. 8(6):8719-29.

[12] Soleimani M, Mahmodi MS, Morsali A, Khani A, Afshar MG. (2011). Using a new ligand for solid phase extraction of mercury. *Journal of hazardous materials*. 189(1-2):371-6.

[13] Esmaeilpour M, Larimi A, Ghahramanafshar M, Faghihi M. (2023). Ethylenediaminetetraacetic acid coated Fe_3O_4@SiO_2 nanocomposite: An effective adsorbent for the removal of copper ions from aqueous system. *Applied Chemistry Today*. 17(65):45-54.

[14] Tufail MK, Ifrahim M, Rashid M, Haq IU, Asghar R, Uthappa U, et al. (2024). Chemistry of zeolites and zeolite based composite membranes as a cutting-edge candidate for removal of organic dyes & heavy metal ions: Progress and future directions. *Separation and Purification Technology*.128739.

[15] Habibi R, Barzegar B, Aghdasinia H, Khataee A. (2024). Enhancement of filtration performance and antifouling properties of polyethersulfone membranes using Fe3O4@ walnut shell-derived activated carbon nanocomposite for heavy metal ions removal. *Journal of Environmental Chemical Engineering*. 12(4):113172.

[16] Nethaji S, Sivasamy A, Mandal A. (2013). Preparation and characterization of corn cob

activated carbon coated with nano-sized magnetite particles for the removal of Cr (VI). *Bioresource technology*. 134:94-100.

[17] Kothavale V, Sharma A, Dhavale R, Chavan V, Shingte S, Selyshchev O, et al. (2023). Carboxyl and thiol-functionalized magnetic nanoadsorbents for efficient and simultaneous removal of Pb (II), Cd (II), and Ni (II) heavy metal ions from aqueous solutions: studies of adsorption, kinetics, and isotherms. *Journal of Physics and Chemistry of Solids*. 172:111089.

[18] Safir I, Ngo KX, Abraham JN, Afshar MG, Pavlova E ,Nardin C. (2015). Synthesis and structure formation in dilute aqueous solution of a chitosan-DNA hybrid. *Polymer*. 79:29-36.

[19] Jin C, Wang Y, Wei H, Tang H, Liu X, Lu T, et al. (2014). Magnetic iron oxide nanoparticles coated by hierarchically structured silica: a highly stable nanocomposite system and ideal catalyst support. *Journal of Materials Chemistry A*. 2(29):11202-8.

[20] Crespo GA, Afshar MG, Barrabés N, Pawlak M, Bakker E. (2015). Characterization of salophen Co (III) acetate ionophore for nitrite recognition. *Electrochimica Acta*. 179:16-23.

[21] Soleimani M, Ghaderi S, Afshar MG, Soleimani S. (2012). Synthesis of molecularly imprinted polymer as a sorbent for solid phase extraction of bovine albumin from whey, milk, urine and serum. *Microchemical Journal*. 100:1-7.

[22] Afshar MG, Crespo GA, Bakker E. (2015). Thin-layer chemical modulations by a combined selective proton pump and ph probe for direct alkalinity detection. *Angewandte Chemie*. 127(28):8228-31.

[23] Wang J, Zheng S, Shao Y, Liu J ,Xu Z, Zhu D. (2010). Amino-functionalized Fe3O4@ SiO2 core–shell magnetic nanomaterial as a novel adsorbent for aqueous heavy metals removal. *Journal of colloid and interface science*. 349(1):293-9.

[24] Xu C, Xu K, Gu H, Zheng R, Liu H, Zhang X, et al. (2 .(‥ٜDopamine as a robust anchor to immobilize functional molecules on the iron oxide shell of magnetic nanoparticles. *Journal of the American Chemical Society*. 126(32):9938-9.

[25] Esmaeilpour M, Javidi J. (2015). Fe3O4@ SiO2-imid-PMAn Magnetic Porous Nanosphere as Reusable Catalyst for Synthesis of Polysubstituted Quinolines under Solvent-free Conditions. *Journal of the Chinese Chemical Society*. 62(4):328-34.

[26] Mahmoodi M, Aslibeiki B, Peymanfar R, Naghshara H, Rajagopal RK, Zhao Y, et al. (2024). Electromagnetic wave absorption performance of Fe3O4/activated carbon-natural resin nanocomposite. *New Carbon Materials*. 39(6):1157-77.

[27] Guan H, Chen Y, Xing K, Liu Q. (2024). Electrochemical sensor based on Fe3O4@ Au/MOF-P2W17V composite modified glassy carbon electrode for food nitrite detection. *Journal of Food Composition and Analysis*. 136:106792.

[28] Niknam E, Naffakh-Moosavy H, Afshar MG. (2022). Electrochemical performance of Nickel foam electrode in Potassium Hydroxide and Sodium Sulfate electrolytes for

supercapacitor applications. *Journal of Composites and Compounds*. 4(12):149-52.

[29] Esmaeilpour M, Ghahraman Afshar M, Kazemnejadi M. (2023). Preparation, characterization, and adsorption properties of bis-salophen schiff base ligand immobilized on Fe3O4@SiO2 nanoparticles for removal of lead(II) from aqueous solutions. *Applied Chemistry Today*. 18(66):125-46. (in persian)

[30] Altalbawy FM, Arbab AM, Makasana J, Jyothi SR, Kumari B, Bhanot D, et al. (2025). Iodine source heterogenized on Fe3O4@ SiO2 modified with dopamine as a green and reusable nanocatalyst for the synthesis of 2, 4, 5-triaryl imidazoles. *Polyhedron*. 268:117355.

[31] Niknam E, Naffakh-Moosavy H, Moosavifard SE, Afshar MG. (2022). Amorphous V-doped Co3S4 yolk-shell hollow spheres derived from metal-organic framework for high-performance asymmetric supercapacitors. *Journal of Alloys and Compounds*. 895:162720.

[32] Bahmaie M, Abbasi L, Faraji M. (2013). Synthesis of magnetic nanoparticles (Fe3O4) and its application for extraction and preconcentration of drug sample from environmental samples. *Applied Chemistry Today*. 8(26):29-37. (in persian)

[33] Zarabadipour M, Soleimani M, Afshar MG. (2025). Application of functionalized Fe3O4@ SiO2 nanoparticles as an adsorbent for heavy metal removal. *Results in Chemistry*.102514.

[34] Weinberger M. (1984). The pharmacology and therapeutic use of theophylline. *Journal of allergy and clinical immunology*. 73(5):525-40.

[35] Vassallo R, Lipsky JJ, editors. Theophylline: recent advances in the understanding of its mode of action and uses in clinical practice. Mayo Clinic Proceedings; 1998: Elsevier.

[36] Persson CG. (1986). Overview of effects of theophylline. *Journal of allergy and clinical immunology*. 78(4):780-7.

[37] Karimi Z, Karimi L, Shokrollahi H. (2013). Nano-magnetic particles used in biomedicine: Core and coating materials. *Materials Science and Engineering: C*. 33(5):2465-75.

[38] Srinivasan SY, Paknikar KM, Gajbhiye V, Bodas D. (2018). Magneto-conducting core/shell nanoparticles for biomedical applications .*ChemNanoMat*. 4(2):151-64.

[39] Kim J-H, Eguchi H, Umemura M, Sato I, Yamada S, Hoshino Y, et al. (2017). Magnetic metal-complex-conducting copolymer core–shell nanoassemblies for a single-drug anticancer platform. *NPG Asia Materials*. 9(3):e367-e.

[40] Asgharinezhad AA, Esmaeilpour M, Afshar MG. (2024). Synthesis of magnetic Fe3O4@ SiO2 nanoparticles decorated with polyvinyl alcohol for Cu (II) and Cd (II) ions removal from aqueous solution. *Chemical Papers*. 78(6):3799-814.

[41] Esmaeilpour M, Ghahraman Afshar M, Kazemnejadi M. (2023). Preparation, characterization, and adsorption properties of bis-salophen schiff base ligand immobilized on Fe3O4@ SiO2 nanoparticles for removal of lead (II) from aqueous solutions. *Applied Chemistry Today*. 18(66):125-46. (in persian)

[42] Esmaeilpour M, Sardarian AR, Firouzabadi H. (2018). Theophylline supported on modified silica-coated magnetite nanoparticles as a novel, efficient, reusable catalyst in green one-Pot synthesis of spirooxindoles and phenazines. *ChemistrySelect*. 3(32):9.٤٨-٢٣٦

[43] Dindarloo Inaloo I, Majnooni S, Eslahi H, Esmaeilpour M. (2020). Air-Stable Fe3O4@ SiO2-EDTA-Ni (0) as an Efficient Recyclable Magnetic Nanocatalyst for Effective Suzuki-Miyaura and Heck Cross-Coupling via Aryl Sulfamates and Carbamates. *Applied Organometallic Chemistry*. 34(8):e5662.

[44] Bai G, Shi L, Zhao Z, Wang Y, Qiu M, Dong H. (2013). Preparation of a novel Fe3O4@ SiO2@ Ni–La–B magnetic core–shell nanocomposite for catalytic hydrogenation. *Materials Letters*. 96:93-6.

[45] Kazemnejadi M ,Rezazadeh Z, Nasseri MA, Allahresani A, Esmaeilpour M. (2019). Imidazolium chloride-Co (iii) complex immobilized on Fe 3 O 4@ SiO 2 as a highly active bifunctional nanocatalyst for the copper-, phosphine-, and base-free Heck and Sonogashira reactions. *Green Chemistry*. 21(7):1718-34.

[46] Suo L, Dong X, Gao X, Xu J, Huang Z, Ye J, et al. (2019). Silica-coated magnetic graphene oxide nanocomposite based magnetic solid phase extraction of trace amounts of heavy metals in water samples prior to determination by inductively coupled plasma mass spectrometry. *Microchemical Journal*. 149:104039.

[47] Gdula K, Gładysz-Płaska A, Cristóvão B, Ferenc W, Skwarek E. (2019). Amine-functionalized magnetite-silica nanoparticles as effective adsorbent for removal of uranium (VI) ions. *Journal of Molecular Liquids*. 290:111217.

[48] Ahmed HA, Soliman MS, Othman SA. (2021). Synthesis and characterization of magnetic nickel ferrite-modified montmorillonite nanocomposite for Cu (II) and Zn (II) ions removal from wastewater. *Egyptian Journal of Chemistry*. 64(10):5627-45.

[49] Ezati F, Sepehr E, Ahmadi F. (2021). The efficiency of nano-TiO2 and γ-Al2O3 in copper removal from aqueous solution by characterization and adsorption study. *Scientific Reports*. 11(1):18831.

[50] Mahdavi S .(٢٠١٦) .Nano-TiO2 modified with natural and chemical compounds as efficient adsorbents for the removal of Cd+ 2, Cu+ 2, and Ni+ 2 from water. *Clean technologies and environmental policy*. 18(1):81-94.

[51] Wang J, Ma X, Fang G, Pan M, Ye X, Wang S. (2011 .(Preparation of iminodiacetic acid functionalized multi-walled carbon nanotubes and its application as sorbent for separation and preconcentration of heavy metal ions. *Journal of hazardous materials*. 186(2-3):1985-92.

[52] Banerjee SS, Chen D-H .(٢٠٠٧) .Fast removal of copper ions by gum arabic modified magnetic nano-adsorbent. *Journal of hazardous materials*. 147(3):792-9.

[53] Lee S-M, Laldawngliana C, Tiwari D. (2012). Iron oxide nano-particles-immobilized-sand material in the treatment of Cu (II), Cd (II) and Pb (II) contaminated waste waters. *Chemical Engineering Journal*. 195:103-11.

[54] Phuengprasop T, Sittiwong J, Unob F. (2011). Removal of heavy metal ions by iron oxide coated sewage sludge. *Journal of hazardous materials*. 186(1):502-7.